Appendix A

NA60's Silicon Pixel Tracker for indium running

This appendix collects two publications related to the NA60 silicon pixel tracker in view of, or as used in, the indium run of 2003. These publications cover hardware, operation and performance aspects. For that reason, it is a very important complement to both chapters 2 and 6.

Section A.1 details work prior to the 2003 indium run, namely individual assembly performance tests and a test-run with three small pixel planes in real experimental conditions which took place in October 2002 with a low-energy lead ion beam.

Section A.2 describes the detector's performance during the indium run in 2003 with emphasis on the accumulated radiation damage and vertexing abilities.

Available online at www.sciencedirect.com
SCIENCE DIRECT®
ELSEVIER
Nuclear Instruments and Methods in Physics Research A 539 (2005) 137–145
NUCLEAR INSTRUMENTS & METHODS IN PHYSICS RESEARCH Section A
www.elsevier.com/locate/nima

Operation and performance of the NA60 silicon pixel telescope

K. Banicz[a,e], A. David[a,b], M. Floris[c], J.M. Heuser[d], M. Keil[a,*], C. Lourenço[a], H. Ohnishi[d], E. Radermacher[a], R. Shahoyan[b], G. Usai[c]

[a]*PH Department, CERN, 1211 Geneva 23, Switzerland*
[b]*Instituto Superior Técnico, Lisbon, Portugal*
[c]*Università di Cagliari and INFN, Cagliari, Italy*
[d]*RIKEN - The Institute of Physical and Chemical Research, Wako, Saitama, Japan*
[e]*Now at Universität Heidelberg, Heidelberg, Germany*

Received 19 May 2004; received in revised form 7 September 2004; accepted 8 October 2004
Available online 19 November 2004

Abstract

The NA60 experiment studies open charm and prompt dimuon production in proton–nucleus and nucleus–nucleus collisions at the CERN SPS. The high multiplicity of charged tracks produced in heavy-ion collisions imposes the use of silicon pixel detectors to perform an efficient tracking. This paper describes the design and assembly of the pixel telescope and performance results from three detector planes operated in the high charged particle multiplicity conditions of Pb–Pb collisions.

PACS: 29.40.Gx; 29.40.Wk

Keywords: Pixel detector; Vertex detector

1. Introduction

The NA60 experiment [1] aims at studying the production of prompt dimuons and open charm in proton–nucleus and heavy-ion collisions at the CERN SPS. New state-of-the-art silicon detectors in the vertex region complement the muon spectrometer and zero degree calorimeter previously used in NA50. A radiation tolerant beam tracker, based on silicon microstrip detectors operated at 130 K, measures the transverse coordinates of the incident ions with a precision of approximately 20 μm. Together with the information from the vertex pixel telescope this allows us to measure the offset of the muon tracks with respect to the event vertex and thereby distinguish events where a pair of D mesons was produced in the collision. So far, the NA60 data taking periods

*Corresponding author. Tel.: +41 22 767 9780; fax: +41 22 767 9487.
E-mail address: markus.keil@cern.ch (M. Keil).

0168-9002/$ - see front matter © 2004 Elsevier B.V. All rights reserved.
doi:10.1016/j.nima.2004.10.019

include proton–nucleus and low energy Pb–Pb collisions in 2002 and high energy In–In collisions in 2003.

2. The NA60 silicon pixel telescope

Downstream of the target and inside a 2.5 T magnetic dipole field, a silicon tracking telescope measures the charged tracks and allows us to identify which of them provide the best match with the muons measured in the muon spectrometer, which is placed behind a hadron absorber. For proton runs, this tracking telescope can consist of silicon microstrip planes, whereas the high particle multiplicity in heavy ion collisions imposes the use of silicon pixel detectors.

The pixel telescope which NA60 developed for the 2003 Indium run consists of 16 independent detector planes with 96 pixel chip assemblies in total, arranged along the beam axis over a length of ~26 cm, starting at ~7 cm downstream of the centre of the target. To optimally subtend the angular acceptance of the muon spectrometer, $3<\eta<4$ or $35<\theta<120$ mrad, the first planes are smaller than the last ones. Fig. 1 shows the arrangement of the pixel detector planes. Each plane consists of several single-chip pixel detector assemblies which are mounted on a planar ceramic support ('hybrid'). The assemblies are made from radiation tolerant, 750 μm thick ALICE1LHCb pixel readout chips [2], bump bonded to 300 μm thick p-on-n silicon pixel sensors with $425\times 50\,\mu m^2$ pixels. The detector planes closest to the target comprise 4 of such assemblies, while the planes further downstream comprise 8 assemblies per ceramic, with two ceramics mounted back-to-back to form one logical plane (Fig. 2). Since the pixel cells are not square, they measure one of the coordinates of the hit, x or y, with a better precision, depending on their orientation when positioned on the planes. To optimise the tracking and vertexing performance of the pixel telescope, the small planes exist in 'x' and 'y' versions, while the large ones are all 'x', having the best resolution coordinate perpendicular to the magnetic field lines, to optimise the momentum measurement. Some planes are placed with

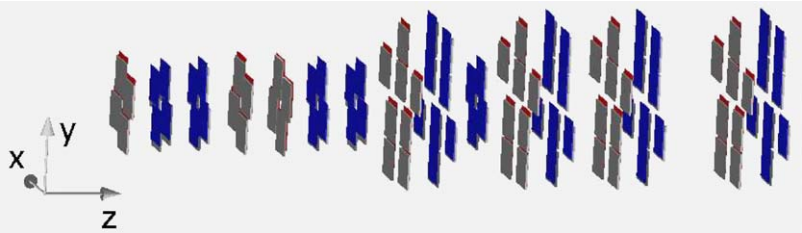

Fig. 1. The complete vertex telescope, consisting of 4-chip and 8-chip planes. The beam comes from the left, the magnetic field is parallel to the y-direction.

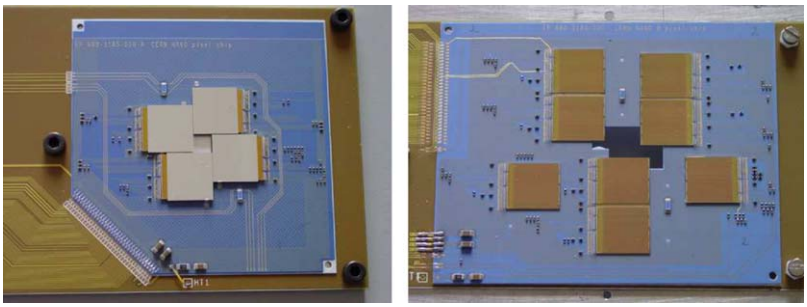

Fig. 2. A 4-chip and an 8-chip hybrid.

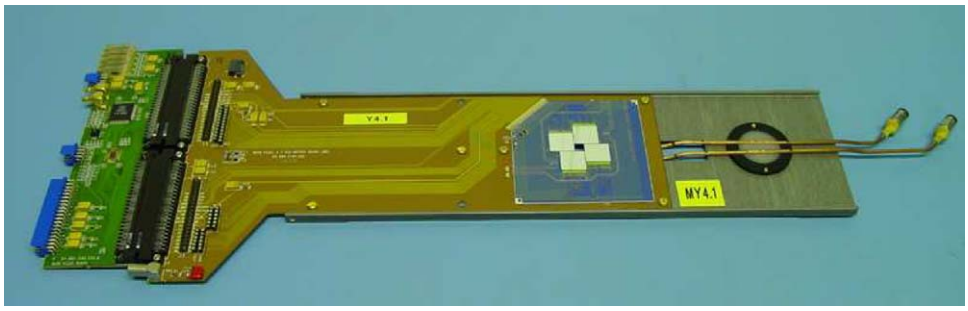

Fig. 3. A 4-chip pixel detector plane with aluminium frame and cooling tubes.

inverted orientation to maximise the overall angular acceptance coverage.

Each of the single chip assemblies consists of a matrix of 32 columns and 256 rows, resulting in a total of 8192 pixels. In the readout chip, every pixel cell contains a preamplifier, a shaper and a discriminator, as well as control and readout logic to transfer the binary hit information to the wire bond pads at the edge of the chip [2]. The collected and amplified charge is digitised by the discriminator whose threshold can be set by a global 8-bit voltage DAC and individually adjusted for each pixel cell by a local 3-bit DAC. Four "test columns" have additional diagnostic outputs at different stages of one readout cell. The chip is operated at 10 MHz and read out over 32 parallel data lines. The chips on one plane are read out sequentially. They were produced in a 0.25 μm technology and have been shown to remain fully functional after exposure to radiation doses of at least 12 Mrad [3]. Therefore, the detector should cope with the radiation levels of ~ 1 Mrad per week expected in the cells closest to the beam axis on the first planes of the NA60 pixel telescope.

The readout chips are glued to the multilayer hybrid circuit fabricated on Al_2O_3 or BeO substrates. The ceramic support itself is glued and wire bonded onto a printed circuit board that provides mechanical support and routes all signals between the front-end electronics and the data acquisition, control and power supply systems. The circuit boards, mounted on aluminium frames, fit into slots of a support box between the dipole magnet shims, defining the detector positions with respect to the targets. The modules are cooled by water at ~12°C circulating in a copper tube attached to the back of the hybrid. Fig. 3 shows a fully mounted 4-chip plane with the aluminium frame and cooling tubes.

3. Tests of assemblies and modules

Prior to the installation in the experiment, comprehensive quality assurance and system tests were performed in the laboratory. Electrical tests and measurements with radioactive sources yielded threshold behaviour, the number of dead pixels and pixels with missing bump connections of the individual assemblies. Assemblies with more than 96% of pixels working were used for the construction of the planes. The assembled planes were then tested and calibrated electrically for the operation in the experiment, using the internal pulser of the readout chip. Maps of dead and noisy pixels were prepared using a ^{90}Sr source.

A common threshold voltage for all pixels in the ALICE1LHCb chip is set by an internal DAC called pre_VTH. The actual threshold value for a given pre_VTH setting is measured by injection of test charges with a varying pulse height. Measuring the response of single pixels as a function of the pulse height gives integrated gaussian distributions whose 50%-point defines the pixel threshold, whereas its width corresponds to the electronics noise. Fig. 4 shows how the measured average threshold depends on the value set on the pre_VTH DAC, for each pixel chip assembly of a given plane. One can see a linear behaviour of the measured average threshold with the pre-set

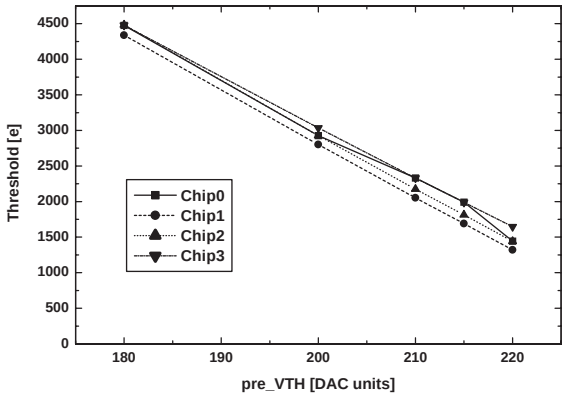

Fig. 4. Threshold calibration for all chips of a pixel detector plane. The measured average thresholds show a linear dependence on the setting of the global threshold DAC. The value of this DAC can be adjusted individually for every chip.

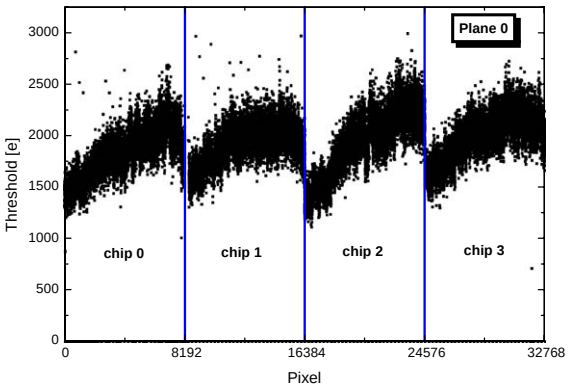

Fig. 5. Measured thresholds for all pixels of a 4-chip plane, for a nominal threshold of 2000 e and without pixel-to-pixel threshold adjustment.

value of the pre_VTH DAC. Thanks to low noise values and small pixel-to-pixel variations of the threshold, a nominal threshold value of 2000 e could be used in the experiment. The measured thresholds for a whole plane at this threshold setting can be seen in Fig. 5. The measurement shown yielded a threshold distribution with a mean value of 1930 e and a width of 260 e. Given the level of signal (approximately 30,000 e average) and of noise ($\sim$ 200 e) a dispersion of 200–300 e on a threshold set at 2000 e does not affect in any visible way the performance of the detector. Therefore, there was no need to use the pixel-to-pixel adjustment, a complex fine tuning procedure, which would have required some effort and a thorough understanding of the sources of the measured threshold dispersion.

4. Results from the 2002 lead ion run

Three 4-chip pixel detector planes were operated in the NA60 experiment during the data taking period of October 2002, when we studied Pb–Pb collisions, at 30 and at 20 GeV per incident nucleon, 5 days at each energy. The target system in this run consisted of three Pb targets of 0.5, 1.0 and 1.5 mm thickness. The pixel detector planes were positioned at 7.8, 10.1 and 13.1 cm downstream from the centre of the target box. Data samples have been collected with two types of triggers, both provided by the zero degree calorimeter of NA60: the "minimum bias" trigger simply required a minimal energy deposited in the calorimeter, to stay above the intrinsic noise of the detector; the "interaction" trigger had the extra condition that this energy was significantly below the total energy of the incident Pb ion, to ensure that an interaction had occurred in the target and the ZDC only measured the energy of the non-interacting beam nucleons. No magnetic dipole field was applied during the data taking.

Fig. 6 shows the number of reconstructed tracks for minimum bias Pb–Pb collisions. A relatively high track density of up to 100 or more tracks per event can be seen, leading to an occupancy of up to 2×10^{-2} hits per pixel per trigger in the pixels close to the beam hole of the detector planes. Fig. 7 shows a typical hit map in one plane, integrated over several minutes.

4.1. Cluster sizes

The behaviour of the cluster sizes has been studied in detail for all three planes since it is directly related to the detector occupancy and could be a limiting factor in forthcoming heavy ion runs.

The collected data sample shows that the cluster size mainly depends on three factors:

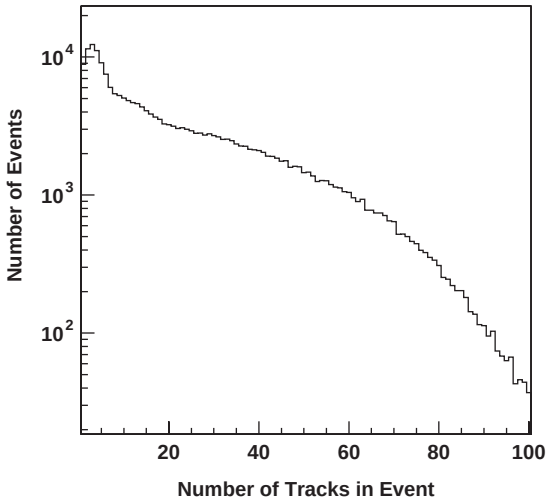

Fig. 6. Distribution of the number of tracks per event reconstructed in the vertex telescope.

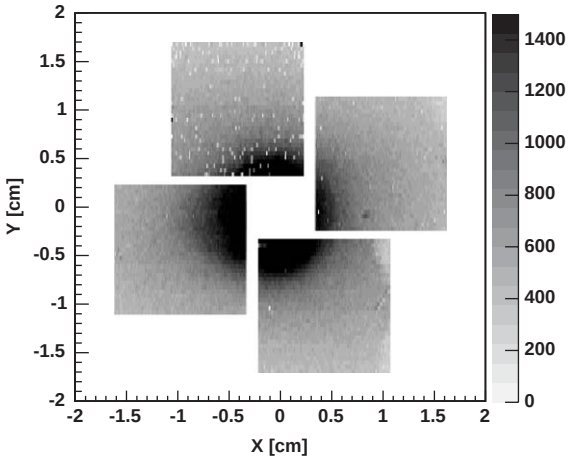

Fig. 7. Hit map of a pixel detector plane integrated over several minutes of Pb–Pb running.

Track angle—Fig. 8 shows the average cluster size versus the slope of the track with respect to the short pixel direction. To exclude the effect of bigger clusters due to delta electrons, clusters of more than three pixels were excluded. The plot shows the behaviour expected from geometrical considerations: with increasing track inclination the number of neighbouring pixels crossed by the particle, and thus the cluster size, increases.

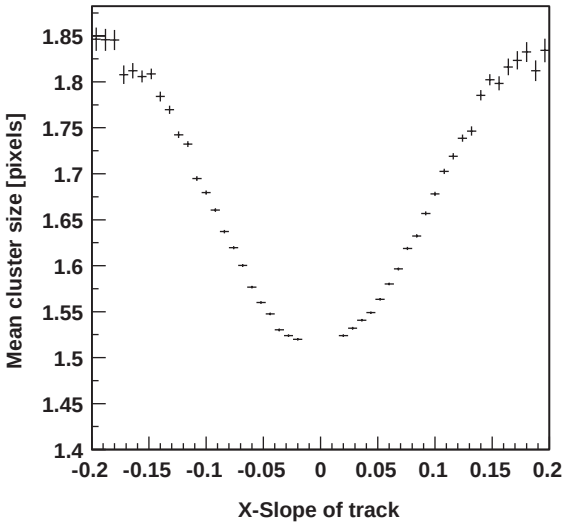

Fig. 8. Dependence of the mean cluster size on the slope of the track, dx/dz, with respect to the short pixel direction. For inclined tracks the charge tends to be deposited in several pixels.

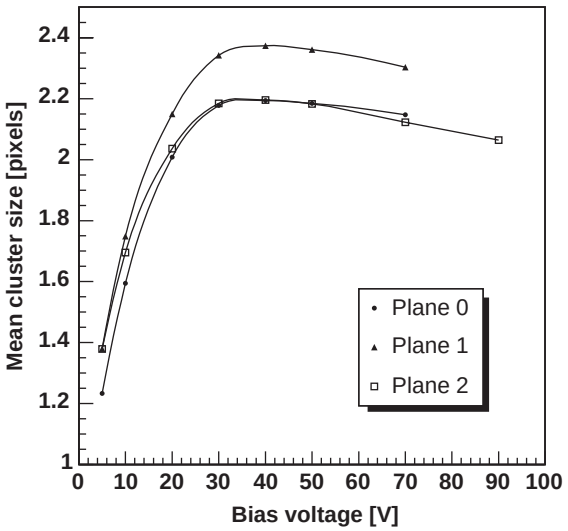

Fig. 9. Dependence of the mean cluster size on the detector bias voltage, for the three planes.

Charge collection—As can be seen from Fig. 9, the average cluster size increases with increasing bias voltage, until the detector reaches the expected point of full depletion (between 30 and 40 V). A further increase of the bias voltage leads

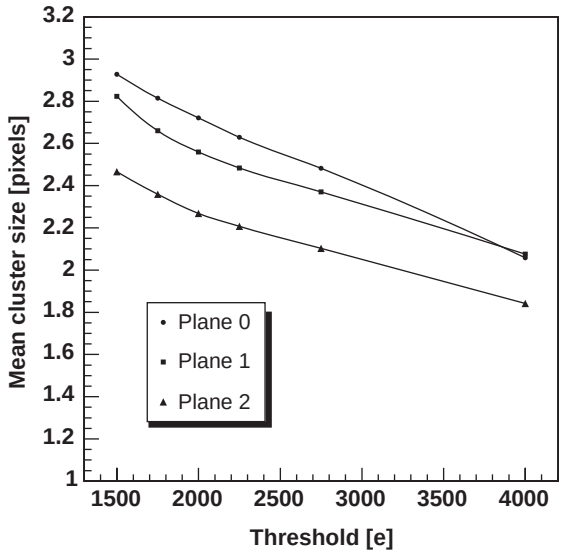

Fig. 10. Dependence of the mean cluster size on the nominal discriminator threshold for all three planes.

to a faster charge collection and to a smaller charge spread parallel to the sensor surface, resulting in a decrease of the cluster size.

Applied threshold—Fig. 10 shows the dependence of the cluster size on the setting of the discriminator threshold. As expected, the cluster size decreases with increasing threshold since, especially in big clusters, many pixels collect only small fractions of the signal charge.

The behaviour of the cluster sizes can, to a good extent, be understood by the effects described above. The threshold setting can be used to lower the occupancy of the pixel planes when necessary, provided the efficiency does not change when increasing the threshold (discussed below).

4.2. Track reconstruction

The spatial resolution and the efficiency of the pixel detector were assessed as follows. In a first step all tracks in the vertex telescope were reconstructed for a given event, requiring that each track has hits in all three planes. After identifying all vertices inside the target region, the vertex with the largest number of attached tracks was chosen. Then a second track reconstruction was done, this time requiring hits in all planes except the one whose efficiency and resolution was to be determined. Furthermore, an attachment to the vertex found in the first step was required, to reduce the combinatorial background. The tracks found in this step were extrapolated onto the plane under study, and that plane was checked for the presence of a hit in the neighbourhood of the extrapolation point. If no cluster could be found within 3σ of the track extrapolation, the chip was considered inefficient for this track.

4.2.1. Efficiency

Fig. 11 shows the efficiencies determined for a single chip versus the y position, corresponding to the chip columns, of the extrapolated track. The efficiency is almost 100% except for the regions of the so-called "test columns", whose efficiency was compromised by non-optimised DAC settings. Excluding the 4 points obviously affected by these columns, we get an average efficiency of 99.0%. No dead or noisy pixels have been excluded from this calculation.

Fig. 12 shows the average efficiency of a complete chip, including the test columns, measured during a threshold scan. We can see that, for thresholds between 1500 e and 4000 e, the efficiency stays constant within the precision of the measurement. This was expected since the average charge of approximately 30,000 e deposited in the sensor is much larger than the thresholds set.

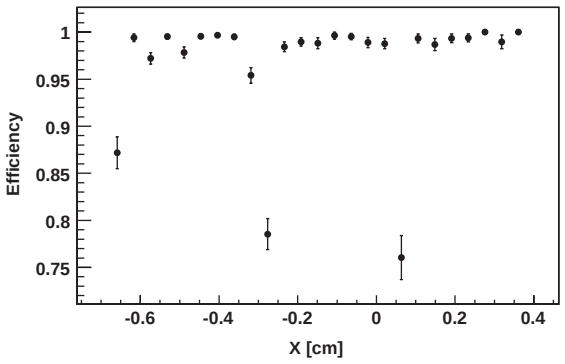

Fig. 11. Efficiency measured for one chip of plane 1. The regions of lower efficiencies are due to the existence of "test columns". Their efficiencies can be much higher when using fine tuned chip settings, not done when the data was taken.

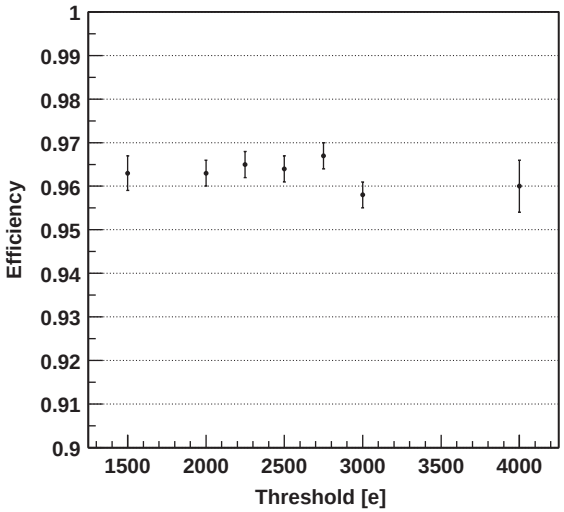

Fig. 12. Dependence of the measured efficiency on the setting of the discriminator threshold. The efficiency has been averaged over the complete chip, including the test columns.

4.2.2. Spatial resolution

Comparing the positions of the extrapolated track points with the hits found in the plane under study yields residual distributions, from which we can derive the spatial resolution. An example of such a distribution is shown in Fig. 13 for the 50 μm pitch direction. The distribution can be described by a convolution of the intrinsic resolution of the pixel plane under study with the resolution function of the track extrapolation. The width of the residual distribution is approximately 13 μm for both 1-pixel and 2-pixel clusters. The contribution of the track resolution was estimated assuming that for a given cluster pattern the spatial resolution is equal in all three planes. Under this assumption we could deconvolute the two contributions, obtaining an intrinsic spatial resolution of approximately 10 μm for both 1- and 2-pixel clusters. At the same time equal numbers of 1- and 2-pixel clusters were observed in the data. This indicates that approximately half of the pixel width contributes to each class, since the ratio between 1-pixel clusters and 2-pixel clusters is directly related to the fraction of the pixel area in which tracks cause single hits or double hits, respectively. This is in agreement with the spatial resolutions measured for both cluster types. The

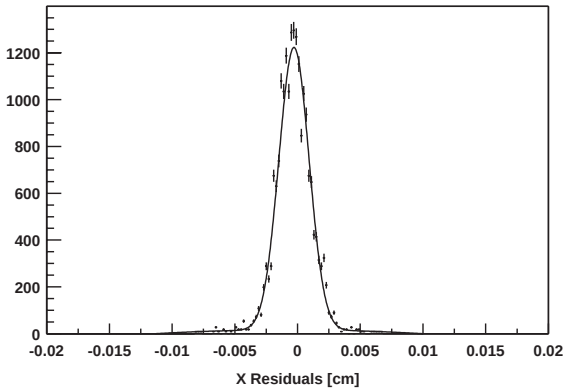

Fig. 13. Residual distribution of 1-pixel clusters in one chip, for the 50 μm pitch direction.

measured value of the resolution is above the theoretical value of $25\,\mu m/\sqrt{12} = 7.2\,\mu m$, where 25 μm is half of the pixel width, which is consistent with an additional contribution of the diffusion width of the charge cloud in the order of 5–7 μm. [1]

4.3. Tracking performance

The tracks measured in the pixel telescope have been used to determine the position of the collision vertices. Fig. 14 shows the distribution of the longitudinal coordinate of the reconstructed vertices. The three Pb targets, as well as the cryostat exit window of the beam tracker, are clearly visible. The distributions for the three targets can be described by a convolution of the target density function and the gaussian resolution function of the vertex reconstruction. Deconvolution leads to the measured thickness of the targets and to the reconstruction resolutions listed in Table 1.

Due to multiple scattering and increasing extrapolation distance, the reconstruction error increases from $\sim$ 200 to $\sim$ 500 μm when going to the most upstream target. The target thicknesses extracted from the deconvolution are in good agreement with the actual values of 1.5, 1.0 and 0.5 mm. The precision of the vertex reconstruction

[1] The value $d/\sqrt{12}$ holds true only for an ideal box distribution. However, in the present case the distribution gets smeared due to the finite diffusion width of the collected charges.

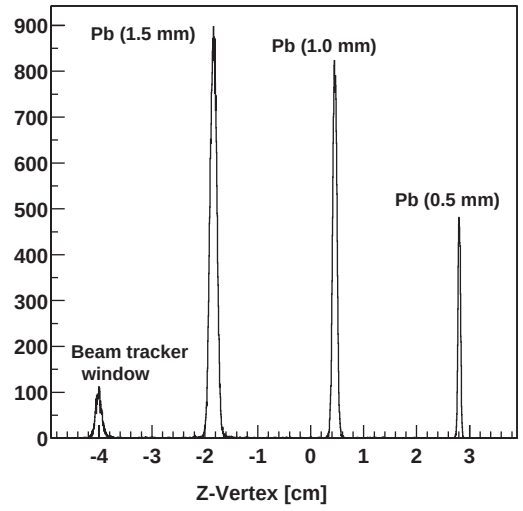

Fig. 14. Z positions of the vertices as measured with the pixel telescope. The peaks correspond to the Pb targets and material from the beam tracker cryostat window.

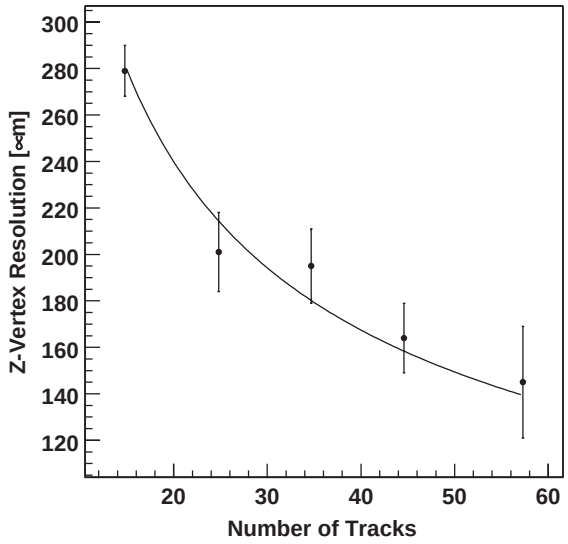

Fig. 15. Z-vertex resolution versus the number of tracks associated with the vertex, for the most downstream target.

Table 1
Z-vertex resolutions and thicknesses of the targets determined from the measured Z-vertex distribution

	Target 1	Target 2	Target 3
Z resolution	0.51 ± 0.01 mm	0.32 ± 0.01 mm	0.21 ± 0.03 mm
Thickness	1.49 ± 0.01 mm	0.98 ± 0.01 mm	0.48 ± 0.02 mm

depends on the number of tracks associated with the vertex, as shown in Fig. 15 for the most downstream target. The plot shows the Z-vertex resolution versus the number of tracks. The data points were fitted with a function of the form

$$\sigma = \frac{\sigma_0}{\sqrt{N_{\text{Tracks}} - 1}} \quad (1)$$

resulting in the value $\sigma_0 = (1050 \pm 30)\,\mu\text{m}$.

Fig. 16 shows the correlation between the x transverse coordinate of the vertex as measured in the pixel telescope and the same coordinate determined with the beam tracker. The correlation width is approximately 30 μm, including the tracking resolution of the beam tracker and the vertex resolution of the pixel telescope. Knowing that the beam tracker gives the transverse coordinates of the interaction point with a resolution

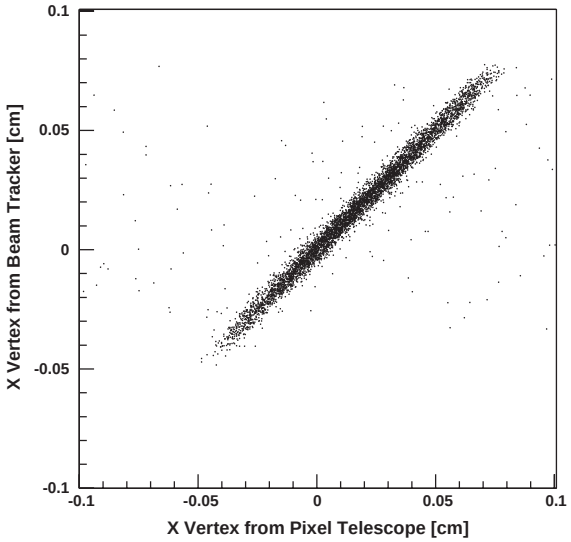

Fig. 16. Correlation between the x transverse coordinate of the vertex measured with the beam tracker and the same variable measured by the pixel telescope.

of ~20 μm, one obtains a transverse vertex resolution of the pixel telescope of approximately 20 μm, for minimum bias collisions. Like the Z-vertex resolution, the transverse coordinate resolution improves for the most central collisions.

5. Summary

The silicon pixel tracking telescope is a crucial detector of the NA60 experiment. In this paper we described the basic concepts determining the detector design, explained the assembly procedure and gave some results from lab tests of chip assemblies and modules. Three 4-chip tracking planes were used in October 2002 to study low energy Pb–Pb collisions. This was the first time that such pixel detectors, based on the Alice1LHCb readout chip, were operated in the high multiplicity environment of heavy-ion collisions. The measurements show that these pixel planes perform extremely well. In the meantime, the full telescope has been completed, and was successfully operated with high energy indium-indium collisions. The corresponding data analysis is ongoing.

Acknowledgements

We would like to express our gratitude to all the people who helped realising this challenging detector on a short time scale. This detector has been developed within the framework of the NA60 experiment. It is therefore natural to start by thanking our colleagues from NA60. In particular, we express our gratitude to D. Marras for help with the electronics aspects of the project. We very much appreciate the crucial contribution from the EP/ED and EP/MIC groups, and from the ALICE pixel project team, especially M. Campbell, P. Riedler, G. Stefanini and K. Wyllie. We also thank E. David, C. Joram, L. Kottelat, I. McGill and A. Onnela, of the EP/TA1 group, for their invaluable help in the design and construction of the pixel telescope. We are also indebted to R. de Oliveira, C. Millerin and M. Sanchez, of the EST/DEM group, for their contribution to the layout and production of the hybrid circuits.

References

[1] A. Baldit, et al., NA60 Proposal, Study of prompt dimuon and charm production with proton and heavy ion beams at the CERN SPS, CERN/SPSC 2000-010, SPSC-P316, March 2000.
[2] K. Wyllie, et al., A pixel readout chip for tracking at ALICE and particle identification at LHCb, Proceedings of the Fifth Workshop on Electronics for LHC Experiments Snowmass, Colorado, 1999, pp. 93–97.
[3] J.J. van Hunen, et al., Irradiation and SPS Beam Tests of the ALICE1LHCb Pixel Chip, CERN-ALI-2001-015, 2001.

Available online at www.sciencedirect.com
SCIENCE DIRECT®
Nuclear Instruments and Methods in Physics Research A 546 (2005) 51–55
NUCLEAR INSTRUMENTS & METHODS IN PHYSICS RESEARCH Section A
www.elsevier.com/locate/nima

The NA60 silicon vertex spectrometer

K. Banicz[a,*], A. David[b], M. Floris[c], J.M. Heuser[d], M. Keil[e], C. Lourenço[e], H. Ohnishi[d], E. Radermacher[e], R. Shahoyan[b], G. Usai[c]

[a]*Universität Heidelberg, Heidelberg, Germany*
[b]*Instituto Superior Técnico, Lisbon, Portugal*
[c]*Università di Cagliari and INFN, Cagliari, Italy*
[d]*RIKEN—The Institute of Physical and Chemical Research, Wako, Saitama, Japan*
[e]*CERN, 1211 Geneva 23, Switzerland*

Available online 31 March 2005

Abstract

The NA60 experiment studies the production of open charm and prompt dimuons in proton–nucleus and nucleus–nucleus collisions at the CERN SPS. To access the kinematics of charged particles already at the vertex level, a radiation tolerant silicon pixel detector has been placed in a 2.5 T magnetic field near the target. This vertex spectrometer was built from 96 ALICE1LHCB pixel chips arranged in 12 tracking planes.

The vertex spectrometer was successfully operated in a run with a 158 GeV/nucleon indium ion beam incident on indium targets in October–November 2003. During the five-week-long run it was exposed to high levels of radiation distributed inhomogeneously over the detector. The most exposed regions of the silicon sensors underwent type inversion.

With only a fraction of the total statistics analysed, the vertex spectrometer can already be seen to have dramatically enhanced the physics performance of NA60 with respect to that of its predecessors.

PACS: 29.40.Wk; 29.40.Gx

Keywords: Silicon pixel detector; Radiation damage

1. Physics program

The NA60 experiment studies extremely hot and dense matter produced in the collisions of ultra-relativistic heavy ions from the CERN SPS accelerator with a fixed target's nuclei. QCD predicts that above a certain temperature or energy density, a phase transition takes place from hadronic matter to Quark Gluon Plasma (QGP), in which quarks and gluons are no longer confined in colorless bound states. In order to gain

*Corresponding author. Tel.: +41 22 767 8670.
E-mail address: Karoly.Banicz@cern.ch (K. Banicz).

0168-9002/$ - see front matter © 2005 Elsevier B.V. All rights reserved.
doi:10.1016/j.nima.2005.03.013

information on this transition, NA60 analyzes the spectrum of the produced dimuons.

Near the phase transition chiral symmetry is expected to be gradually restored, possibly leading to observable changes of the shape of the ρ meson in the dimuon spectrum. For these changes to be seen, the resonances must be resolved at different collision centralities. This requires a good momentum resolution and high statistics.

The most direct evidence of the thermal equilibrium of the QGP would be the observation of thermal dimuons. In the intermediate mass region, the other known contributions to the dimuon spectrum are from the Drell–Yan process and the semileptonic decay of charmed mesons, which are long-lived enough to travel appreciable distances from the interaction vertex before decaying. The tracks of muons originating from charmed meson decays are thus displaced by a few hundred microns from the interaction vertex. Separating them from the prompt thermal dileptons calls for an excellent vertexing precision.

In the plasma the bound $c\bar{c}$ states (e.g., J/ψ or χ_c) should be dissolved, resulting in their suppression with increasing collision centrality. Counting them at different collision centralities demands high statistics.

2. Detector concept

Before hitting the target, the beam particles are tracked by a cryogenic silicon strip detector. This beam tracker measures the transverse coordinates of the interaction vertex with 20 μm precision. Placed in a 2.5 T magnetic field, the silicon vertex spectrometer tracks all produced charged particles within the muon spectrometer's acceptance. The hadron absorber can only be traversed by highly energetic muons, whose coordinates and momenta are measured by the muon spectrometer. Two muon spectrometer tracks pointing to the interaction region are required for the trigger. By matching the momentum vectors of the tracks in the vertex spectrometer with those in the muon spectrometer, we can identify which two of the hundreds of tracks in the vertex spectrometer were the muons. Measuring the charged particles' coordinates and momenta at the vertex and identifying the muons among them makes it possible to determine accurately the vertex position, to reject muons from kaon and pion decays, to measure the offset of the muons originating from charmed meson decays, and to refine the measurement of the muon momenta.

As dimuon production is a rare process, very high luminosity is needed to obtain high statistics. The high charged particle multiplicity of high-energy nuclear collisions imposes the use of high-granularity and radiation-tolerant silicon pixel detectors for the tracking in the interaction region.

3. The vertex spectrometer

The vertex spectrometer consists of eight 4-chip planes and eight 8-chip planes (Fig. 1). The 4-chip planes, which are in the upstream half, each cover the whole acceptance of the detector, whereas it takes a pair of 8-chip planes to do so. Altogether they give 12 space points for tracking. The first plane is at 7 cm from the target, the last one at 33 cm. The chips are glued onto a ceramic hybrid, whose back side is fitted with a cooling pipe, in which cold water is circulated.

Each pixel chip is an assembly of a sensor chip and a frontend readout chip. Both the sensor chip and the frontend readout chip have a matching 32×256 matrix of $425 \times 50\,\mu m^2$ pixels. The two are held together by 25 μm solder bumps connecting each sensor pixel with its corresponding readout pixel. The sensor chip is fabricated from 300 μm thick, high resistivity (15 kΩ cm) n-type bulk with p-type pixel implants. The 750 μm thick readout chip [1] is manufactured in 0.25 μm CMOS technology, and has an enclosed gate geometry and special guard rings, resulting in improved

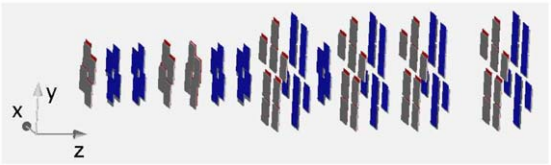

Fig. 1. The 96 chips of the vertex spectrometer arranged in 16 planes. The beam is in the direction of the Z-axis.

radiation tolerance [2]. It was designed by the CERN Microelectronics Group for the ALICE and LHCb experiments.

The detector is operated at 10 MHz. As the interactions occur randomly during 5 s long bursts, the 2-cycle-long trigger gate must be resynchronized to the clock. The 32 columns of a chip are read out in parallel, and the chips on a plane sequentially.

4. Operation

The detector was operated in 2003 in a 5-week-long run. During this time 6×10^{12} indium ions hit the 20% interaction length indium target. The resulting fluences were both simulated with FLUKA [3] and Venus [4], and measured during the first 3 weeks with *pin* diodes and Al activation. Fig. 2 shows the strong inhomogeneity of the radiation.

The temperatures and leakage currents were permanently monitored throughout the run. The total leakage current on a 4-chip plane increased typically from a few microamperes at the beginning to a hundred microamperes at the end of the run (Fig. 3). This corresponds to about 20 nA in the most exposed pixels, still well below the 100 nA limit of the preamplifier's leakage current compensation.

Radiation also decreases the effective doping concentration, and the n-type bulk eventually

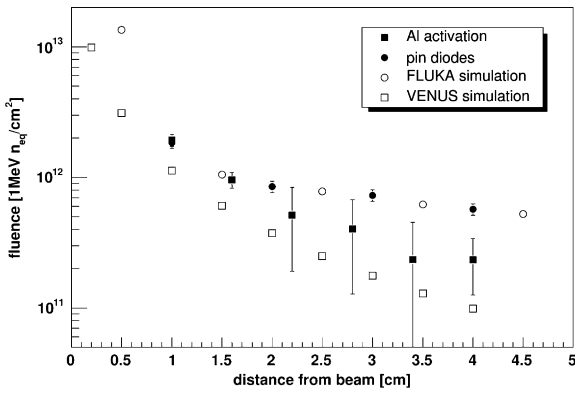

Fig. 2. The simulated and measured fluences 40 cm downstream of the target as a function of the radial distance from the beam.

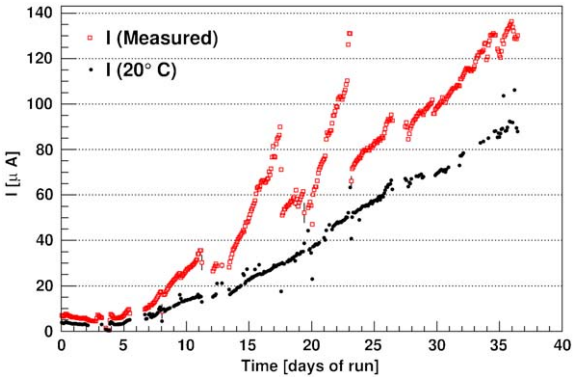

Fig. 3. History of the leakage current during the run on a 4-chip plane (squares). The spikes were caused by temperature rises due to deteriorating cooling, which needed to be repaired repeatedly. The solid circles show the leakage current scaled to a constant temperature.

becomes p-type. As a consequence, after type inversion the rectifying junction moves from the implants to the back plane, and the detector must be fully depleted in order to prevent the pixels from being short-circuited. Since after type inversion the depletion voltage increases with the fluence, pixels in the more exposed inner region need a higher bias voltage to function properly. This effect was observed in a bias scan in the fourth week of the run (Fig. 4).

In future, by use of these pixel chips the effect of the increasing leakage current will be kept under control by operating them at lower temperatures; however the rising depletion voltage will eventually exceed the device's breakdown voltage of about 300 V. This is expected to happen after an accumulated fluence of 4×10^{13} $1\mathrm{MeVn_{eq}/cm^2}$ if annealing effects are neglected. As a result an even larger central area will be left not fully depleted resulting in a loss of angular acceptance for the detector.

5. Performance

The vertexing precision in the Z coordinate (parallel to the beam) is obtained from the resolution of the targets' shape (Fig. 5). It is found to be about 300 μm, using on average fifty tracks to reconstruct a vertex. In the transverse plane the

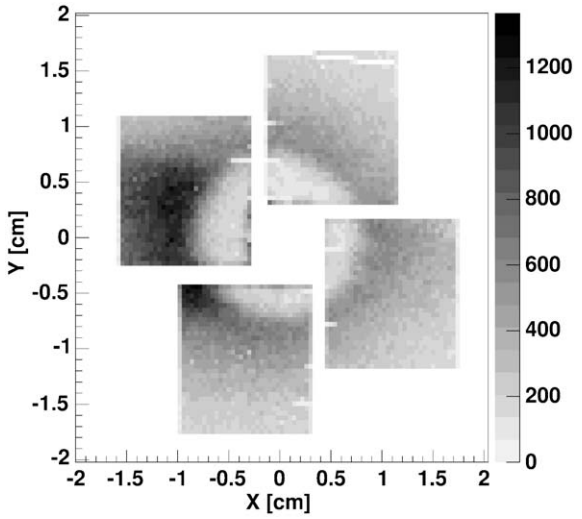

Fig. 4. Distribution of hits accumulated over 20 thousand events on a 4-chip plane during a bias voltage scan done in the fourth week of the run. The depletion voltage in the central part has already risen above the 30 V applied here, rendering the pixels inefficient in that area.

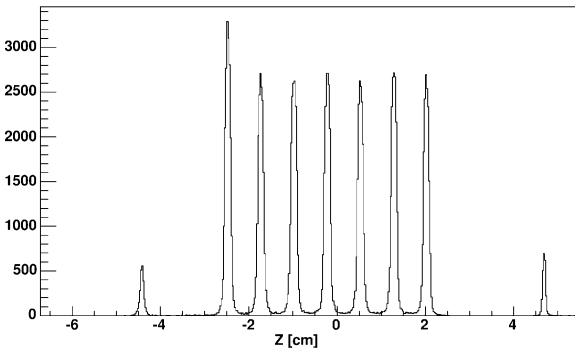

Fig. 5. The vertex distribution along the Z-axis. Visible are the thin vacuum windows of the target box and the seven indium targets, each a 1.5 mm thick cylinder. The front target diameter is larger than the others.

beam tracker already measures the position with a known resolution. From the comparison of the positions given by the the beam tracker and the vertex spectrometer, a resolution of 20 μm is inferred.

The vertex spectrometer measures the momenta of the muons before they suffer considerable energy loss and multiple scattering in the hadron absorber. Combining this information with the muon spectrometer measurement leads to a dimuon mass resolution unprecedented in heavy-ion collisions. (Fig. 6) [5].

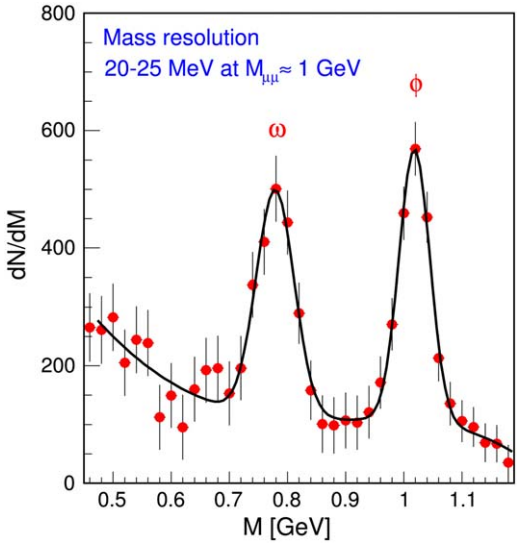

Fig. 6. The dimuon invariant mass spectrum in a small subsample of the indium–indium data after combining the measurements by the pixel and muon spectrometers, and subtracting the background. From the measured widths of the ω and ϕ resonances a resolution of 20−25 MeV is inferred. The resolution of the muon spectrometer measurement alone is ~80 MeV.

6. Summary

NA60 has successfully operated a silicon pixel detector in a high-rate and high-multiplicity environment. The detector has met the requirements of high speed, high granularity and radiation tolerance dictated by a broad and ambitious physics program. The chips have been exposed to fluences up to 5×10^{13} 1MeVn$_{eq}$/cm^2 and undergone type inversion. They are still operational and will be essential for the proton-nucleus physics run of 2004.

References

[1] K. Wyllie, presentation at this Workshop.

[2] W. Snoeys, et al., Nucl. Instr. and Meth. A 466 (2001) 366.
[3] A. Fassò, et al., eConf C0303241, MOMT004 (2003) [arXiv:physics/0306162].
[4] K. Werner, Phys. Rept. 232 (1993) 87.
[5] P. Sonderegger, et al., [NA60 Coll.], J. Phys. G 30 (2004) S1027;
H. K. Wöhri, et al. [NA60 Coll.], First results on Dimuon production from the NA60 experiment, Frascati Phys. Series 34 (2004) 185.
R. Arnaldi, et al. [NA60 Coll.], Rencontres de Moriond, QCD and Hadronic Interactions, 2004, hep-ex/0406054, to be published.